MYCOLOGIA

Mycologia

ISSN: (Print) (Online) Journal homepage: https://www.tandfonline.com/loi/umyc20

A precise relationship among Buller's drop, ballistospore, and gill morphologies enables maximum packing of spores within gilled mushrooms

Martina Iapichino, Yen-Wen Wang, Savannah Gentry, Anne Pringle & Agnese Seminara

To cite this article: Martina Iapichino, Yen-Wen Wang, Savannah Gentry, Anne Pringle & Agnese Seminara (2021) A precise relationship among Buller's drop, ballistospore, and gill morphologies enables maximum packing of spores within gilled mushrooms, Mycologia, 113:2, 300-311, DOI: 10.1080/00275514.2020.1823175

To link to this article: https://doi.org/10.1080/00275514.2020.1823175

Published online: 26 Jan 2021.

MYCOLOGIA
2021, VOL. 113, NO. 2, 300–311
https://doi.org/10.1080/00275514.2020.1823175

Taylor & Francis
Taylor & Francis Group

A precise relationship among Buller's drop, ballistospore, and gill morphologies enables maximum packing of spores within gilled mushrooms

Martina Iapichino[a], Yen-Wen Wang[b,c], Savannah Gentry[b,c], Anne Pringle[b,c], and Agnese Seminara[a]

[a]Institut de Physique de Nice, UMR7010, Centre National de la Recherche Scientifique (CNRS) and Université Côte d'Azur, Nice, France; [b]Department of Botany, University of Wisconsin–Madison, Madison, Wisconsin 53706; [c]Department of Bacteriology, University of Wisconsin–Madison, Madison, Wisconsin 53706

ABSTRACT

Basidiomycete fungi eject basidiospores using a surface tension catapult. A fluid drop forms at the base of each spore and, after reaching a critical size, coalesces with the spore and launches it from the gill surface. It has long been hypothesized that basidiomycete fungi pack the maximum number of spores into a minimal investment of biomass. Building on a nascent understanding of the physics underpinning the surface tension catapult, we modeled a spore's trajectory away from a basidium and demonstrated that to achieve maximum packing the size of the fluid drop, the size of the spore, and the distance between gills must be finely coordinated. To compare the model with data, we measured spore and gill morphologies from wild mushrooms and compared measurements with the model. The empirical data suggest that in order to pack the maximum number of spores into the least amount of biomass, the size of Buller's drop should be smaller but comparable to the spore size. Previously published data of Buller's drop and spore sizes support our hypothesis and also suggest a linear scaling between spore radius and Buller's drop radius. Morphological features of the surface tension catapult appear tightly regulated to enable maximum packing of spores. If mushrooms are maximally packed and Buller's drop radii scale linearly with spore radii, we predict that intergill distance should be proportional to spore radius to the power 3/2.

ARTICLE HISTORY
Received 25 July 2019
Accepted 10 September 2020

KEYWORDS
Ballistospory; biomechanics; fungi; morphometrics

INTRODUCTION

Molds, yeasts, and mushrooms are ubiquitous across Earth. Estimates of the number of fungal species range from 1 to more than 5 million (Blackwell 2011), and fungi in ecosystems function as decomposers, mutualists, and pathogens. Emerging fungal diseases endanger crops as well as wild plants and animals, threatening food security, but fungal diseases also alter forest dynamics and contribute to the extinction of animals. Losses cost millions of US dollars in damage (Pennisi 2010; Fisher et al. 2012; Kupferschmidt 2012).

Most fungal bodies (mycelia) are immobile, typically hidden within substrates. Fungi use spores to reproduce and travel away from a natal habitat. Spores are carried in air currents away from a source, and when a spore lands in a favorable environment, it germinates and begins or extends the life cycle. Basidiomycota are among the most common fungi, encompassing pathogens such as the honey mushroom as well as charismatic mushrooms such as matsutake and the fly agaric. The phylum is defined by the production of sexually derived spores (basidiospores) on a basidium. Basidiospores are launched via a surface tension catapult. Among species of mushroom-forming fungi, e.g., agarics and boletes, spores typically form in groups of four from basidia arranged along the gills or pores of a mushroom, each spore attached to a sterigma. A drop of liquid, known as Buller's drop, forms extracellularly at the base of each spore when water condenses on the hilar appendix of a spore. Buller's drop then collapses onto another adaxial drop formed along the longitudinal axis of the spore itself (FIG. 1).Upon coalescence, surface energy is converted into kinetic energy. The spore is ejected horizontally away from the basidium and sterigma. The spore decelerates to rest after a few milliseconds and then falls vertically between two gills or within the pore.

Ballistospore discharge was first observed by Schmitz (1843). In the 20th century, Buller (1909) described the phenomenon in more detail, observing the discharge of the spore and describing both the formation of the drop at the hilar appendix and the subsequent launch of the spore together with the drop. The drop is now referred to as "Buller's drop" and the discharge understood as a "surface tension catapult." We also use the phrase "spore-drop complex" to mean the entire spore discharge complex, including the adaxial drop, Buller's

CONTACT Agnese Seminara agnese.seminara@unice.fr

Published online 26 Jan 2021

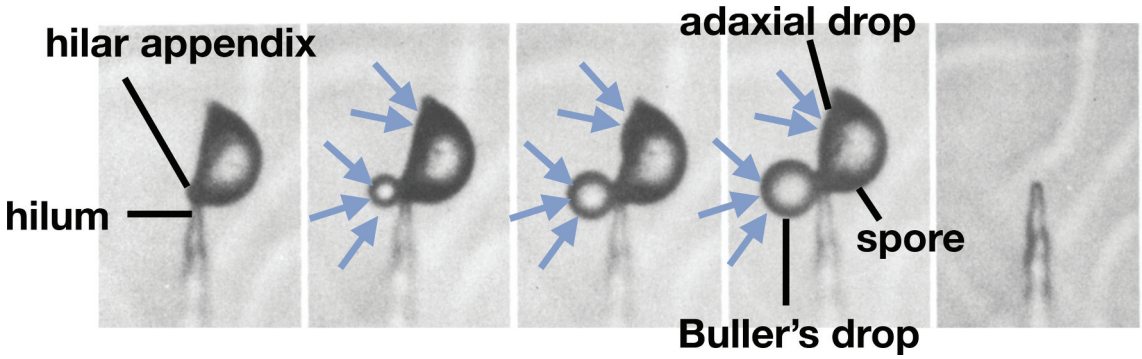

Figure 1. Our current understanding of the surface tension catapult. Left to right: Spore and structure holding spore; Buller's drop forms and grows by condensation at the base of the spore (blue arrows). At the same time, the adaxial drop (visible to some extent in the central frame and indicated by blue arrows) grows on the surface of the spore, also by condensation (blue arrows). At a critical size, Buller's drop collapses onto the adaxial drop and reduces the total liquid surface, thus releasing energy. The released energy is converted into kinetic energy, catapulting the spore away from its parent. The size of Buller's drop, together with material parameters, determines the speed of spore discharge. Image adapted from Webster et al. (1984).

drop, and the spore. Progress in understanding the anatomy and physics of the surface tension catapult was enabled by the development of cameras. Webster et al. (1984) provided photographic evidence of Buller's drop forming at the hilar appendix just before discharge and proposed a two-phase mechanism for spore ejection: the first phase involved Buller's drop enveloping the spore surface, acquiring momentum; the second entailed the sharing of momentum and movement of the center of mass of the spore-drop complex, a result of rapid wetting. Subsequent works modeled the conversion of surface energy into kinetic energy with different degrees of complexity and imaged ballistospore launch with progressively faster cameras (Pringle et al. 2005; Noblin et al. 2009; Stolze-Rybczynski et al. 2009; Fischer et al. 2010b; Liu et al. 2017). Pringle et al. (2005) observed coalescence, whereas Noblin et al. (2009) described the process as encompassing four stages and estimated that approximately half of the total surface energy was dissipated during launch. Recently, Liu et al. (2017) moved beyond considerations of energy balance to generate simulations of the fluid dynamics within the Buller's drop and the adaxial drop during coalescence and described experiments with biomimetic drops. These authors found that coalescence occurs in a regime where viscous dissipation in the Buller's drop is negligible. Hence, energy is not dissipated to set Buller's drop in motion; instead, it may be dissipated to break the spore from the sterigma. In addition, Liu et al. (2017) found that the phenomenon known in physics as "pinning" of the contact line (de Gennes 1985) provides directionality for the spore-drop complex as it ejects away from the originating gill.

It has long been hypothesized that mushrooms form gills to increase the surface area for spore production and pack the maximum number of spores into a minimal investment of biomass (Buller 1909; McKnight and Roundy 1991; Fischer and Money 2010). To achieve an optimal morphology, the size of Buller's drop, the size of the spore, and the distance between gills must be finely coordinated. Whereas spore size and intergill distance may be under genetic control (Kues and Liu 2000), Buller's drop forms extracellularly (Webster et al. 1989). Whether and how fungi control the size of Buller's drop remains unknown, although data reporting characteristic sizes of Buller's drop for different species suggest individual species do control size (Pringle et al. 2005; Stolze-Rybczynski 2009; Stolze-Rybczynski et al. 2009; Fischer et al. 2010b).

To explore whether the morphologies of gilled mushrooms enable the maximum packing of spores within tissues, we first revisit the theory relating ejection velocity and flight time to the horizontal distance traveled by a spore from the moment of launch to the moment it begins settling underneath the gills (Buller 1909; Pringle et al. 2005; Noblin et al. 2009; Stolze-Rybczynski et al. 2009; Fischer et al. 2010b; Liu et al. 2017). Using energy balance, we obtain the ejection speed and highlight its dependence on the sizes and densities of the spore and Buller's drop. Combining expressions for ejection speed and flight time, we predict the distance traveled ballistically by the spore-drop complex before downward sedimentation starts. We then use our model to elucidate the criteria enabling maximum packing of spores. In the phase space made up of the three variables: (i) drop radius, (ii) spore radius (defined as the radius of a sphere with the same volume as the spore), and (iii) intergill distance, the criterion for maximum packing is that spores must travel ballistically exactly midway between two facing gills. Given two of the three variables (i) to (iii), the model predicts the third, assuming maximum packing. To compare our model with empirical data, we collected mushrooms of eight different species and

measured spore size and intergill distance. By placing these morphological data on the phase space generated from our model, we predict that for collected species, the radius of Buller's drop that maximizes spore packing ranges between 23% and 50% of the radius of the spore (depending on the precise value of spore density and efficiency of energy conversion). To validate the prediction, we revisit previously published data for an additional 13 species (Pringle et al. 2005; Stolze-Rybczynski 2009; Stolze-Rybczynski et al. 2009; Fischer et al. 2010b) and find Buller's drop scales as 32% of spore size, consistent with our prediction. These results suggest that Buller's drop radius scales linearly with spore radius and, combined with our model, generate a second prediction: to enable maximum packing, intergill distance should be proportional to spore radius to the power 3/2. In the aggregate, our work synthesizes thinking about the morphologies of Buller's drop, spores, and gills, while providing insights into the principles shaping ballistospory.

MATERIALS AND METHODS

Spore ejection speed.— The reduction in surface energy following coalescence is $\sim\pi\gamma R_B^2$, where γ is surface tension of Buller's drop and R_B is Buller's drop radius. By balancing the surface energy to the kinetic energy of the spore-drop complex, $1/2(m_s + m_B)v_0^2$, we obtained

$$v_0 = \sqrt{\frac{2\pi\gamma\alpha\, R_B^2}{m_s + m_B}} \tag{1}$$

where v_0 is the ejection velocity and m_s and m_B are the mass of the spore and of Buller's drop. Note that we have neglected viscous dissipation because ballistospory operates in a regime of low Onhesorge number (Liu et al. 2017). By simple algebra, we can express v_0 in the following form:

$$v_0 = U\sqrt{\frac{y^2}{y^3 + \beta}}$$

where $U = \sqrt{3\alpha\gamma/(2\rho_B R_s)}$ is a velocity scale independent of Buller's drop radius; R_s is the radius of a sphere with the same volume as the spore—this is the "equivalent radius" of the spore, and we will call it "spore radius" for short; $y = R_B/R_s$ is the normalized Buller's drop radius, i.e., the ratio of Buller's drop to spore radii; ρ_B and ρ_s are densities of Buller's drop and spore, respectively; and $\beta = \rho_s/\rho_B$ is the ratio of spore to Buller's drop densities. The parameter α accounts for the fraction of available energy dissipated when the spore breaks apart from the hilum, the point of attachment between the spore and the sterigma (FIG. 1).

Relaxation time of the spore-drop complex.— The complex's relaxation time is determined by the air drag that causes rapid deceleration and is well approximated by the Stokes time (Stokes 1851; Fischer et al. 2010a):

$$\tau = \frac{2R^2}{9\bar{\beta}\nu} \tag{2}$$

where ρ_a, ρ_s, and ρ_B are the densities of air, spore, and Buller's drop, respectively; $\bar{\beta} = \rho_a\left(R_s^3 + R_B^3\right)/(\rho_S R_s^3 + \rho_B R_B^3)$ is the density of air divided by the density of the spore-drop complex; ν is the kinematic viscosity of air; and R is the radius of the spore-drop complex, which we consider to be a sphere with volume equal to the sum of the spore and drop volumes: $R = \left(R_B^3 + {R_s}^3\right)^{\frac{1}{3}}$. When Buller's drop is considerably smaller than the spore, which is often the case, $\bar{\beta}\sim\rho_a/\rho_s$. Following simple algebra, we obtain the Stokes time of the spore-drop complex in the following nondimensional form:

$$\tau = T\left(y^3 + 1\right)^{\frac{2}{3}}$$

where $T = \frac{2{R_s}^2}{9\nu\bar{\beta}}$, and ν is the kinematic viscosity. The list of the parameters used in the model is listed in TABLE 1, together with their estimated or measured values from the literature.

Data collection and published data.— Between 15 and 17 Sep 2017, we collected mushrooms from the Upper Peninsula of Michigan. On 15 Oct 2017, we collected mushrooms from the University of Wisconsin–Madison Lakeshore Natural Preserve. We collected opportunistically, taking any mushroom that appeared in good shape but focusing on gilled (not pored) fungi. We collected specimens of eight morphologically distinct species (TABLE 2).

We also retrieved published data from the literature; these data were generated from a different group of species (TABLE 3) and provide measurements of Buller's drops and spores but do not provide information about intergill distances (Pringle et al. 2005; Stolze-Rybczynski 2009; Stolze-Rybczynski et al. 2009; Fischer et al. 2010b). In this series of papers, the authors captured ballistospory from high-speed video microscopy and obtained Buller's drop and spore sizes (but not intergill distance) from image analysis. We discarded the species for which measurements of Buller's drop size were inferred indirectly. When spore volume was available, spore radius was calculated as $R_s = \left(\frac{3V_s}{4\pi}\right)^{1/3}$. When spore volume was not available directly, we calculated it from spore length and width, assuming spores are prolate spheroids,

$V_s = \frac{4}{3}\pi L_s W_s^2$. Values of spore density range from 0.8 to 3.8 g/cm^3 (Hussein et al. 2013).

Data from the literature were used to estimate the efficiency parameter α as follows. For two species of basidiomycota (*Auricularia* and *Sporobolomyces*), for which geometry of the spore and Buller's drop was observed directly, the velocity of ejection was 73% and 68% of the theoretical maximum (Noblin et al. 2009), yielding fractions of usable energy of $0.73^2 = 0.53$ and $0.68^2 = 0.46$; hence, α = 50 ± 5%, consistent with estimates presented in Stolze-Rybczynski (2009), based on a different hypothesis about the geometry of the adaxial drop.

Preparing specimens for morphometrics.—On the same day mushrooms were collected, a scalpel was used to separate caps from stems (FIG. 2A). Caps were left face down for 8 to 12 h on a piece of paper covered with aluminum foil in order to create spore prints (FIG. 2B). Spore prints are generated when spores fall from gills and settle directly underneath the cap. Spore prints reflect the morphology of each collected specimen, and the location of stems and patterns of gill spacing are easily seen from a spore print. To image spores, three small pieces of foil, each measuring approximately 1 mm × 1 mm, were cut (i) from close to each stem, (ii) equidistant between the stem

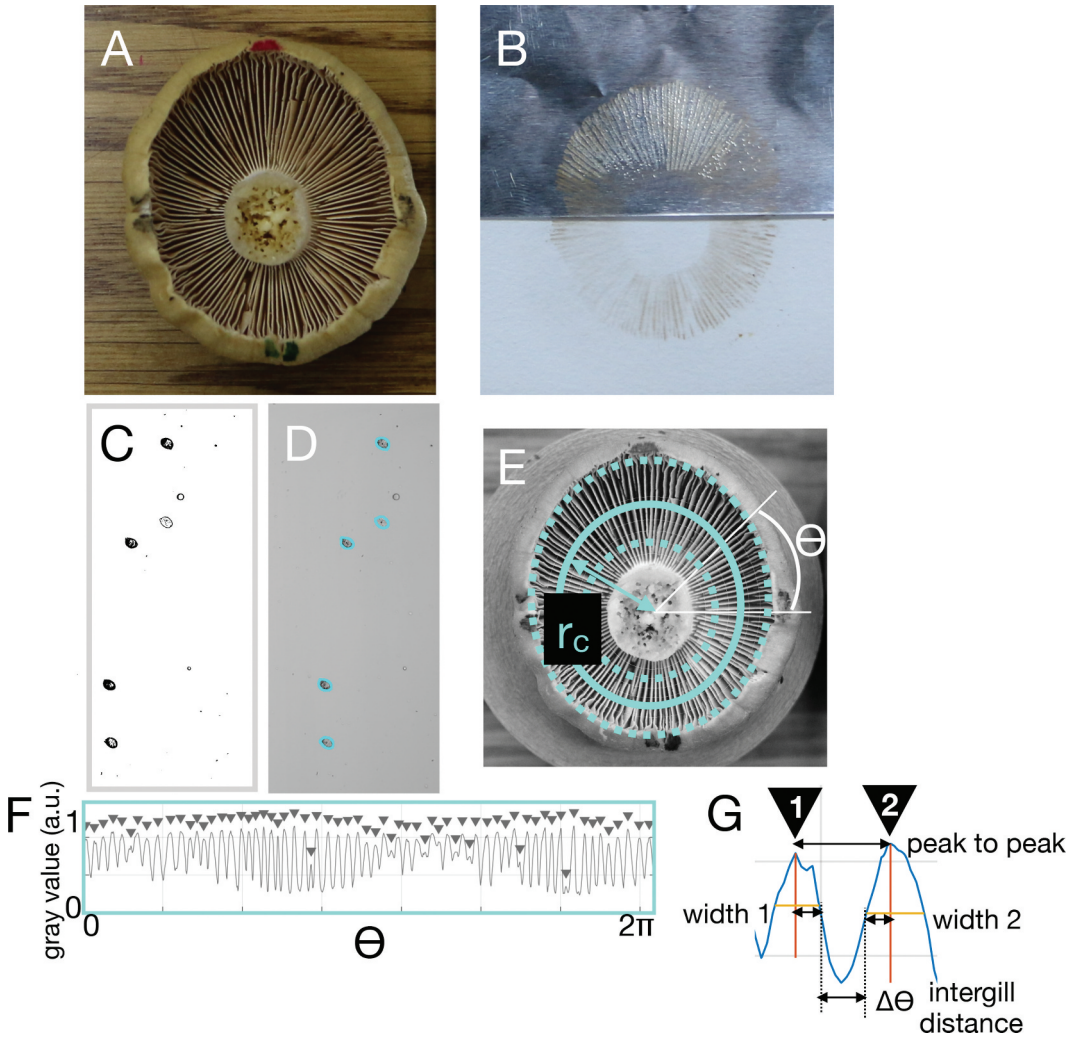

Figure 2. Collection and analysis of gill spacing in wild mushrooms. A. An image of the underside of a mushroom cap collected fall 2017 in Michigan. B. Spore print obtained by placing the spore cap on half aluminum foil/half paper overnight. C. Confocal microscope image of a sample of spores from the spore print. D. Segmentation of image, used to recover spore contours. E. Concentric circles around the center of the cap mark where intergill distances were measured and define the azimuthal angle θ, used to compute intergill distance. F. Grayscale values from image in E, as a function of azimuthal angle θ. Peaks correspond to gills (white in the image of E), whereas troughs correspond to the spaces between gills (dark or black in the image of E). To obtain intergill distance, we marked all peaks (note arrows) and kept track of their azimuthal angles. G. Close-up image showing locations of two peaks, marked by arrows 1 and 2. Intergill distance $\Delta\theta$ is defined in radiants, as the peak-to-peak distance (difference in azimuthal angle of two adjacent peaks) minus the width of the gills themselves (width 1 and width 2; see Materials and Methods). We calculated intergill distances in mm by multiplying $\Delta\theta$ for the radius of the circle (r_c in E).

and the cap edge, and (iii) from near the edge of each cap. Spores were washed off each foil piece and suspended in a 0.01%vol solution of Tween 80. Fifteen microliter of each spore suspension was immediately spread onto a glass slide and spores imaged. Microscope slides were sealed with nail polish to minimize evaporation of the Tween solution and prevent the movement of spores during imaging. To measure distances between gills, a photograph of each cap's underside, with a ruler included in the photograph, was taken immediately after spore printing using a Canon EOS400D camera (Canon Inc., Japan).

Identification of species using DNA barcoding.— Tentative field identifications were confirmed by sequencing the nuc rDNA internal transcribed spacer region ITS1-5.8S-ITS (ITS barcode; Schoch et al. 2012) of each mushroom. To generate DNA barcodes for each collected mushroom, we extracted DNA with an NaOH extraction method modified from Wang et al. (1993). First, the tissues of each sporocarp were ground finely with a pestle in 40μL of 0.5 M NaOH and the solution centrifuged at 13 000 rpm for 10 min. Five microliter of supernatant was transferred to 495 μL of 100 mM Tris-HCl (pH 8) and centrifuged at 13 000 rpm for another minute. Next, the resulting supernatant was used as template for polymerase chain reaction (PCR). We amplified the ITS using primers ITS1F (Gardes and Bruns 1993) and ITS4 (White et al. 1990) following PCR protocols outlined in White et al. (1990) modified for Lucigen's EconoTaq Plus Green 2× Master Mix (Lucigen, Middleton, Wisconsin).

Amplified products were cleaned and then Sanger sequenced by Functional Biosciences (Madison, Wisconsin). Sequences were deposited in GenBank under accession numbers MK829236–MK829244. Two specimens, one *Mycena* (MK829242) and one *Russula* (MK829243), could not be confidently identified to species despite their barcode data.

Microscopy and image analysis to measure spore geometry.— Images of spores were taken using microscopes housed at the Newcomb Image Center at the University of Wisconsin–Madison. Spores were imaged either individually or in groups (FIG. 2C), depending on whether a particular microscope's field of view housed one or more than one spore, using Zeiss Elyra LSM 780 and Zeiss LSM 710 confocal microscopes (Carl Zeiss AG, Germany). Spores were not stained, as all collected species proved to be autofluorescent. The laser wavelength used to excite autofluorescence was 405 nm. The average area S and average radius of spores $R_s = \sqrt{S/\pi}$ of each species were then calculated from images of between 155 and 1180 spores using an image analysis tool implemented in ImageJ 1.51. A single pixel's dimension in μm was calculated from the microscope and the images converted to grayscale (8-bit or 16-bit). ImageJ was then used to threshold each image and convert the grayscale to a binary image, highlighting all the spores to be counted and using the measurement of a single pixel to calculate the area of each spore, as shown in FIG. 2C–D. Spores touching other spores were not measured, nor were particles smaller than 2 μm^2. Particles bigger than 2 μm^2 were identified either as spores or not by eye.

Image analysis to measure intergill distances.— To measure distances between gills, we first identified the center of each cap by eye (FIG. 2E). We then drew between 6 and 10 circles (depending on the size of each specimen's cap) concentrically around the center of the cap (FIG. 2E). We then used ImageJ 1.51 (National Institutes of health, Bethesda, Maryland) to open each picture, set pixel length in mm using the image of the ruler included in each photograph, and convert images to grayscale (8-bit or 16-bit). The Oval Profile plugin was used to obtain grayscale profiles traced along each of the concentric circles drawn onto an image.

Profiles were sampled at 3600 equally spaced points along each circle. Next, the area of each circle was measured to calculate its average distance from the cap center, and these measurements were later used to convert the distance between gills from radiants to mm. The grayscale profile obtained from ImageJ along each circle was imported into MATLAB R2017b (Natick, Massachusetts; one example in FIG. 2F) and analyzed with the function Findpeaks. Peaks in the grayscale image identify the centers of gills, which appear white in grayscale images. Peaks that were closer than 0.3° were discarded as noise. We visually inspected data to confirm that minor peaks did correspond to gills. Finally, we quantified gill thickness as the width of the peak, defined as the distance where gray value drops half way below peak prominence, which is a measure of peak height. The distance between two gills, d, was defined as the distance between their centers minus the half-width of each of the two gills (see close-up of two peaks in FIG. 2G).

RESULTS

Ejection speed.— We first focused on the velocity achieved by the surface tension catapult, which depends on various physical parameters as well as on the dimensions of the spore and Buller's drop. Let us first recapitulate the physical processes that lead to spore launch. Buller's drop coalesces with the adaxial drop to power the surface tension catapult; both drops are made from condensed water vapor and appear following the

secretion of hygroscopic substances by the fungus. When Buller's drop coalesces with the adaxial drop, the resulting reduction of surface area provides the surface energy to accelerate the spore. Because the adaxial drop is pinned to the surface of the spore, Buller's drop accelerates along the axis of the spore toward its distal tip. Once the moving drop reaches the tip of the spore, capillarity and contact line pinning decelerate water, and its momentum is transferred to the spore. Momentum transfer causes the force that breaks the contact between the spore and the sterigma, resulting in spore ejection away from the basidium.

In this physical process, surface energy is converted in kinetic energy; by using the physical principle of energy conservation, we obtained EQUATION 1 (see Materials and Methods): this equation predicts that there will be a radius of Buller's drop that maximizes v_0 (FIG. 3A). By zeroing the derivative in EQUATION 1, we obtained the size of Buller's drop that maximizes ejection speed: $y_{max} = (2\beta)^{1/3}$, and when considering spores with densities once to twice the density of water (Hussein et al. 2013), β = 1–2. This equation implied that at y_{max}, Buller's drop radius is comparable to the equivalent radius of the spore $R_B \sim 1.26R_s$ to $1.59R_s$ (the gray shade in FIG. 3A marks all values of y_{max}, for β ranging from 1 to 2). Note that at y_{max}, control of the ejection speed is robust, i.e., ejection speed becomes insensitive to small deviations from the exact value of Buller's drop size. Buller's drop is generally assumed to scale with spore length (Fischer et al. 2010b), and this scaling appears to hold for at least 13 species of basidiomycetes, as shown in Pringle et al. (2005), Stolze-Rybczynski (2009), Stolze-Rybczynski et al. (2009), and Fischer et al. (2010b). FIG. 3B uses these published data to calculate spore radius R_s, pointing to $y_{literature} = R_B/R_s \sim 0.32 \pm 0.08$, where we report the best fit through the data and $\pm$ the mean residual. $y_{literature}$ values are represented in cyan on the horizontal axis in FIG. 3A, suggesting these fungi do not operate at maximum ejection speed, but rather remain on the rising slope well away from the maximum, different from other species (see Fritz et al., 2013). Note that only 3 out of their 13 species were gilled mushrooms (TABLE 3), but these 3 species lined up with the rest of the data and showed no clear departure from the rest of the collected data (FIG. 3B).

Ballistic range.—In order to understand how far a spore-drop complex travels after launch, we analyzed the timescale τ over which the spore-drop complex decelerates to rest, or relaxation time (see Materials and Methods). We found that after discharge, spores travel horizontally a distance given by

$$x = v_0\tau$$

with v_0 and τ from EQUATIONS 1 and 2. Next, a spore stops abruptly and starts to sediment vertically, out from beneath a pair of facing gills, following a trajectory commonly known as a "sporabola" (FIG. 4A).

Maximum spore packing.—In order to successfully escape the mushroom, a spore must travel away from its basidium a distance x into the clear space between gills before settling downward; it must travel far enough to avoid entrapment within the basidia and spores underneath it. If x is in fact dictated by this criterion that ensures spores escape the gills without sticking to

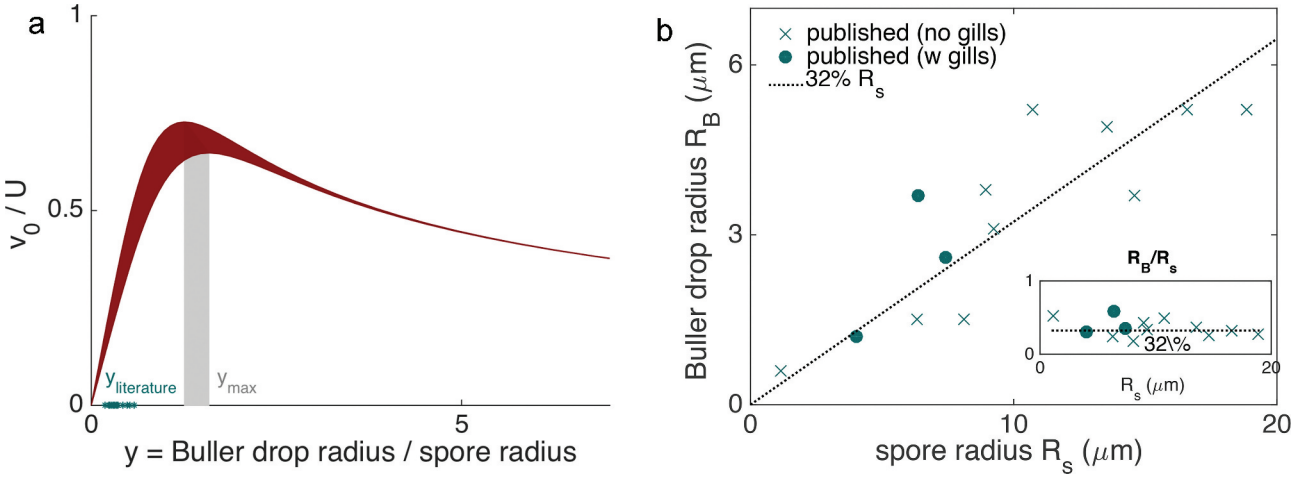

Figure 3. A. Energy balance from EQUATION 1 predicts discharge speed. We represent the normalized speed, v_0/U, as a function of y, defined as the ratio of Buller's drop radius, R_B, divided by spore radius, R_s (red line). The thickness of the red line represents predicted speed for β ranging from 1 to 2, where β is the ratio of spore to drop densities. B. Linear scaling between spore radius and Buller's drop radius from data published in the literature (see TABLE 3). Spore radius is calculated as described in the main text.

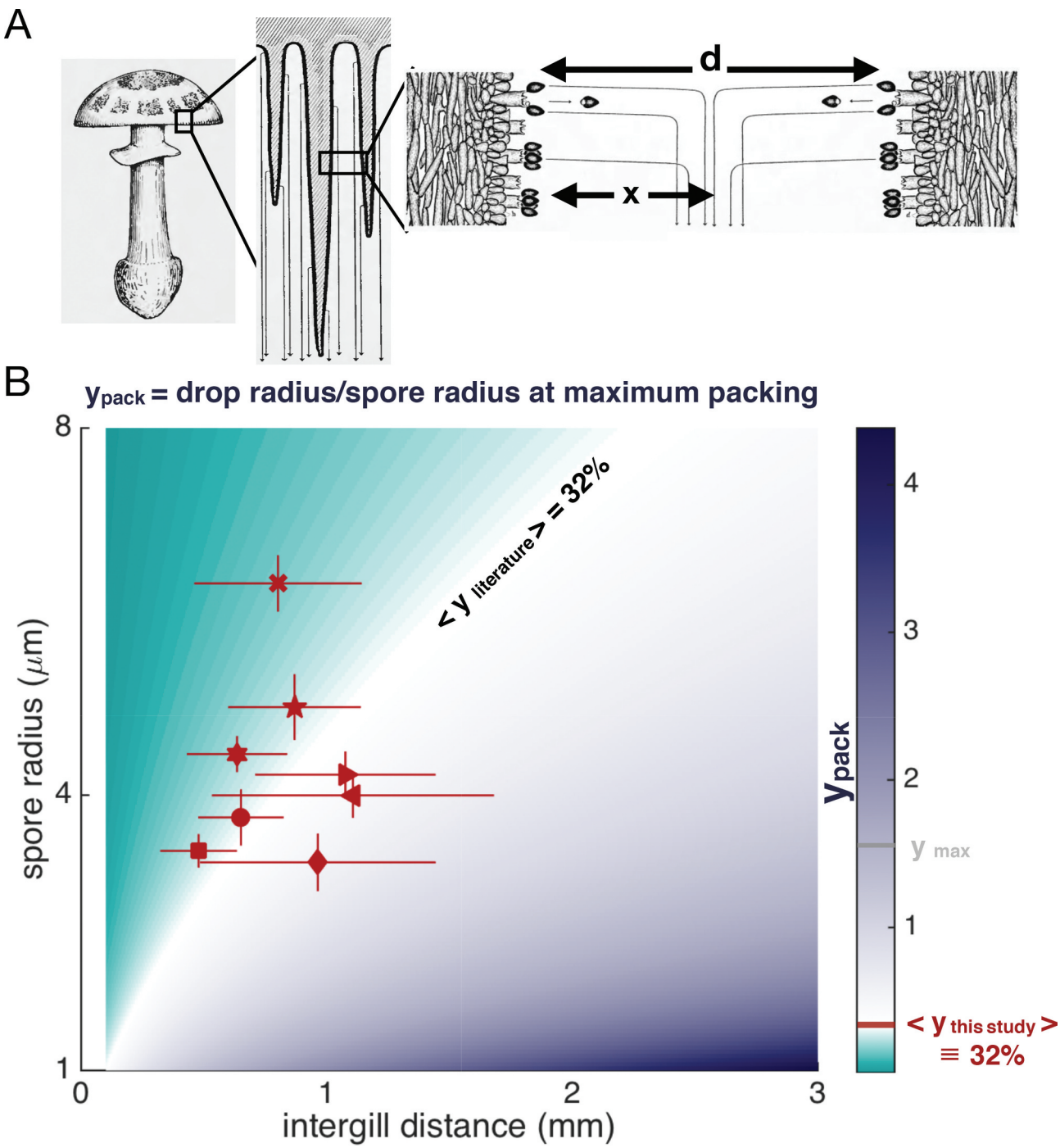

Figure 4. Mushroom cap morphology and the maximum packing of spores. A. From left to right: Representative mushroom; detail of gill arrangement indicating sporabolas (trajectories of individual spores); magnified view of adjacent gills with basidia and basidiospores. Sporabolas are represented in faint gray in the center panel and black arrows in the right panel; adapted from Buller's drawing (Buller 1909). Maximum packing implies that spores initially travel a distance $x = v_0\tau$ to reach the midpoint between two facing gills separated by $d = 2v_0\tau$, with v_0 and τ given by EQUATIONS 1 and 2. B. Prediction for normalized Buller's drop radius at maximum packing, y_{pack}, obtained by numerically solving EQUATION 3 with the parameters listed in TABLE 1. y_{pack} is color-coded from 0 (cyan) to 4.4 (black); white corresponds to the value $y_{\text{literature}} = 32\%$. Symbols correspond to data of intergill distances and spore radii measured from eight species collected by us in Michigan and Wisconsin. Each symbol is linked with a species as in FIGS. 5 and 6 and TABLE 2. The optimal Buller's drop radius for the eight collected species is $y_{\text{pack}} \sim 0.32 \pm 0.12$, where we report average $\pm$ standard deviation. The free parameters a and ρ_s are chosen within their range of natural variation. The prediction varies little across the range of variation of a and ρ_s.

tissue underneath, and assuming all gills are reproductive, then the distance between two facing gills, d, should be at least twice x, hence $d > 2x$. To pack as many spores as possible within a mushroom and avoid inefficient empty spaces, the distance between gills must be close to this minimum value:

$$d = 2x$$

where $x = v_0\tau$. Maximum packing was first suggested by Buller (1909), and this relationship appeared explicitly in more recent literature (Stolze-Rybczynski et al. 2009). Plugging in the values of v_0 and τ given by EQUATIONS 1 and 2, we obtain

$$\left(\frac{y_{\text{pack}}^2}{y_{\text{pack}}^3+\beta}\right)^{1/2}\left(y_{\text{pack}}^3+1\right)^{2/3} = \frac{d}{2UT} \qquad (3)$$

where U and T are the velocity and timescale derived in the previous two paragraphs and summarized in TABLE 1 and y_{pack} is the normalized Buller's drop radius; we add the subscript $_{\text{pack}}$ to stress that this prediction is valid at maximum packing. EQUATION 3 predicts the relationship between three variables: nondimensional Buller's drop radius y_{pack}, spore radius R_s (R_s is contained in the expressions for U and T summarized in TABLE 1), and intergill distance d—at maximum packing. Hence, given two of these three variables, EQUATION 3 predicts the third, assuming maximum packing and given the values of the parameters (spore density, energy conversion efficiency). For example, for any combination of spore radius and intergill distance, EQUATION 3 predicts the optimal radius of Buller's drop that achieves maximum packing. We solve EQUATION 3 numerically and show the result for the normalized radius of Buller's drop, y_{pack}, in FIG. 4, color-coded from 0 (cyan) to 5 (black) for different combinations of intergill distances and spore radii using parameters listed in TABLE 1. At each point in the phase space defined by spore radius and intergill distance, the color represents the value of normalized Buller's drop radius that achieves maximum packing. Symbols and error bars represent our own data, described, analyzed, and discussed below.

Data collection.— To compare our model with data, we measured spore and gill morphologies (see Materials and Methods) for eight wild mushroom species (TABLE 2). Whereas spore size varied from species to species, spores within a single mushroom cap were considerably more similar and there were

Table 1. List of parameters and their estimated or measured values from the literature.

Parameter	Symbol	Value	Reference	Value used in FIG. 3
Air density	ρ_a	1kg/m^3		1kg/m^3
Spore density	ρ_s	0.8 to 3.8 g/m^3	Hussein et al. 2013	1.8 g/m^3
Buller's drop density	ρ_B	1 g/m^3	Same as water[a]	1 g/cm^3
Buller's drop surface tension	γ	0.07 N/m	Same as water[a]	0.07 N/m
Efficiency of energy conversion	α	50 ± 5%	Noblin et al. 2009	0.5
Spore to Buller's drop density ratio	$\beta = \rho_s/\rho_B$			
Air to Buller's drop density ratio	$\bar{\beta} = \rho_a/\rho_B$			
Reynolds number	$Re_B = R_s\gamma/(\nu^2\rho_B)$			
Reynolds number	$Re_s = R_s\gamma/(\nu^2\rho_s)$			
Intergill distance	d			
Spore radius	R_s			
Buller's drop radius	R_D			
Normalized Buller's drop radius	$y = R_B/R_s$			
y at maximum packing	y_{pack}			
Time scale	$T = 2R_s^2/(9\nu\bar{\beta})$			
Velocity scale				

[a]Webster and coauthors estimated that Buller's drop contains about 1% in mass of mannitol and sucrose (Webster et al. 1995); hence, γ and ρ_B are well approximated by the surface tension and density of water (Hoorfar et al. 2006).

Table 2. List of collected species, collection locations, numbers of spores imaged and analyzed, and corresponding symbols used in the figures.

Collected species	Location	No. spores analyzed	Symbol
Camarophyllus borealis	Marquette County, Michigan	231	▶
Cortinarius caperatus	Marquette County, Michigan	1180	✸
Amanita lavendula	Marquette County, Michigan	155	✖
Armillaria mellea complex (A)	Marquette County, Michigan	301	★
Armillaria mellea complex (B)	Marquette County, Michigan	257	◀
Mycena sp.	UW-Madison Lakeshore Natural Preserve, Wisconsin	530	●
Russula sp.	UW-Madison Lakeshore Natural Preserve, Wisconsin	1053	◆
Galerina marginata	UW-Madison Lakeshore Natural Preserve, Wisconsin	1159	■

Table 3. Data of Buller's drop radius and spore radius from the literature.

Species (order or class)	Spore-bearing structure	R_B (μm)	L_S (μm)	W_S (μm)	V_S (μm)	R_S (μm)	Refernce
Trametes versicolor (Polyporales)	Pores	0.6	—	—	6.4	1.15	Fischer et al. 2010b
Aleurodiscus oakesii (Russulales)	Smooth, discoid	5.2	23.2	17.0	—	18.86	Pringle et al. 2005
Itersonilia perplexans (Tremellales)	Yeast	4.9	15.1	12.8	—	13.52	Pringle et al. 2005
Tilletiopsis albescens (Exobasidiomycetes, incertae sedis)	Yeast	3.7	13.4	4.4	—	6.38	Pringle et al. 2005
***Laccaria amethystina* (Agricales)**	Gills	1.5	8.1	8.1	—	8.1	Stolze-Rybczynski 2009
Stereum hirsutum (Russulales)	Pores	1.2	7.2	3.0	—	4.02	Stolze-Rybczynski 2009
***Xerula radicata* (Agaricales)**	Gills	3.7	16.8	13.6	—	14.59	Stolze-Rybczynski 2009
Gymnosporangium juniperi-virginianae (Pucciniales)	Gelatinous telial horns	5.2	20.0	15.1	—	16.58	Stolze-Rybczynski 2009
Tilletia caries (Tilletiales)	Host tissue	5.2	21.4	7.6	—	10.73	Stolze-Rybczynski 2009
Sporobolomyces salmonicolor (Sporidiobolales)	Yeast	3.8	11.5	7.9	—	8.95	Stolze-Rybczynski 2009
Auricularia auricula (Auriculariales)	Smooth, jelly-like	3.1	12.9	7.8	—	9.22	Stolze-Rybczynski 2009
Polyporus squamosus (Polyporales)	Pores	2.6	14.0	5.4	—	7.41	Stolze-Rybczynski 2009
***Armillaria tabescens* (Agaricales)**	Gills	1.5	6.8	6.1	—	6.32	Stolze-Rybczynski 2009
Clavicorona pyxidata (Russulales)	Smooth, coral-like	1.2	4.7	3.5	—	3.86	Stolze-Rybczynski 2009

Note. R_B = Buller's drop radius; L_S = spore length; W_S = spore width; V_S = spore volume; R_S = spore equivalent radius. Species that produce gilled mushrooms are in boldface.

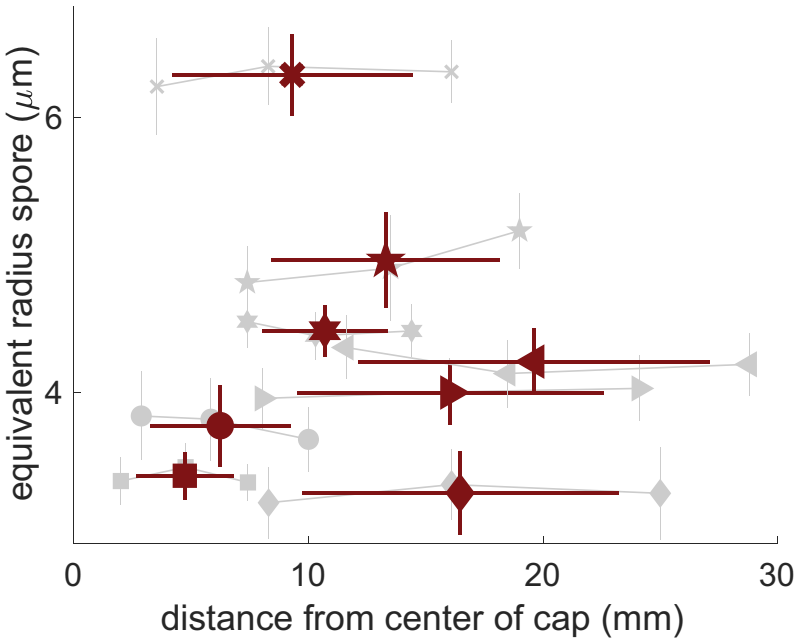

Figure 5. Spore size does not vary across a single mushroom cap. Gray thin lines mark measurements of spore radius taken at three different distances from cap stipes, with error bars representing standard deviations; means and standard deviations for spore radius at all distances are shown in dark red vertical lines. Horizontal red line guides the eye.

no consistent pattern of variation, e.g., spores were not larger nearer the center or edge of a cap (FIG. 5). Moreover, the average intergill distance also remains constant with distance from the center of the cap. The phenomenon is driven by the appearance of secondary gills (lamellulae) toward the edge of a mushroom cap; as two gills with origins at the stipe diverge, often a secondary gill will appear. The appearance of secondary and tertiary gills keeps intergill distances constant. The only species in our data set with variable intergill distances was an unidentified species of *Russula*, which did not produce secondary gills (Phillips 1991; Fischer and Money 2010). Among measured species, intergill distances

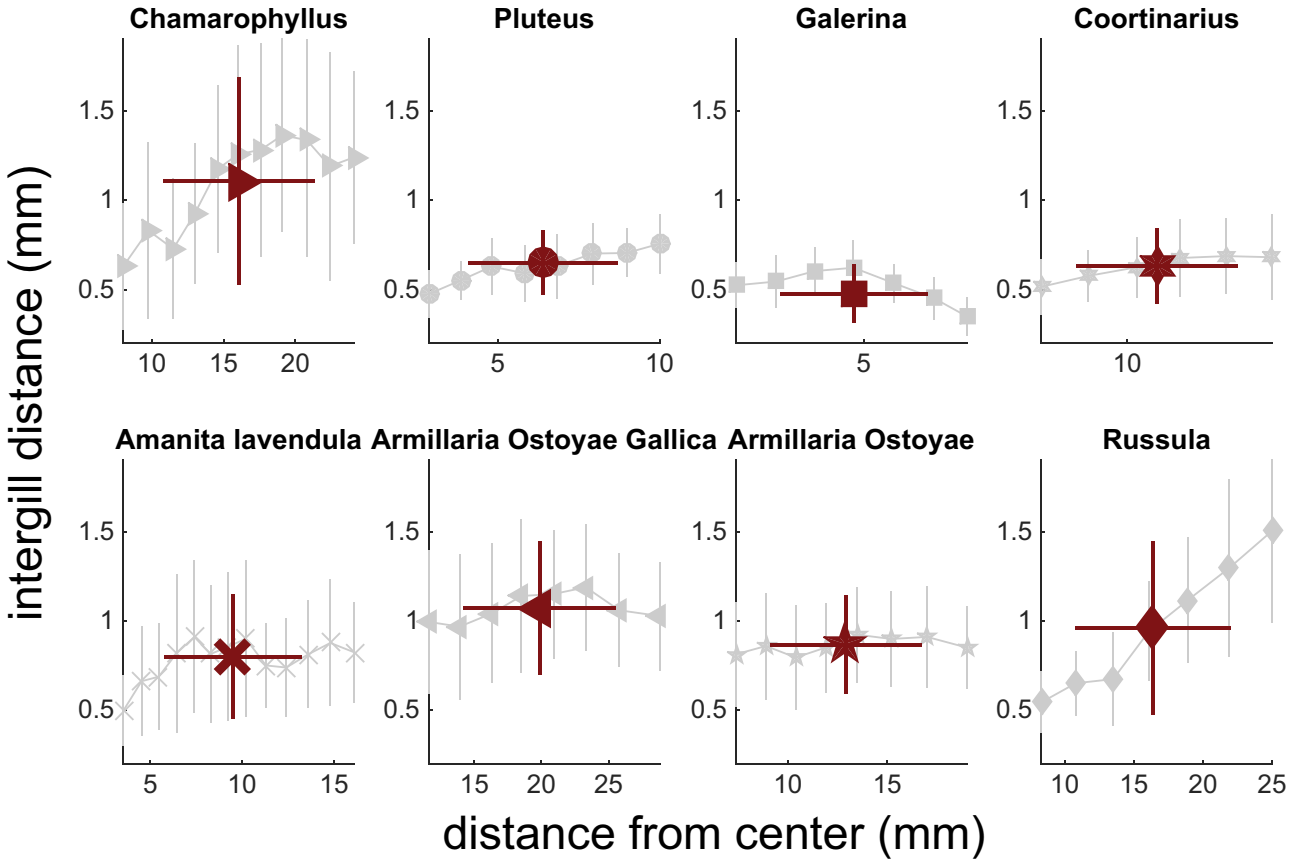

Figure 6. Average gill spacing varies little with distance from cap stipes, a result driven by the appearance of secondary gills at greater distances from the cap stipe. Gray lines show all measurements at various distances from the center; vertical red lines show the average values and standard deviations. Horizontal red line guides the eye. The only exception is *Russula* sp., which has no secondary gills.

varied from about 0.25 mm to 1.5 mm(FIG. 6), but there was no obvious correlation between intergill distances and the size of the mushroom cap.

To ensure maximum packing in real species, we predicted that Buller's drop radius should be 23% to 50% of spore radius.— Here, we used EQUATION 3 and data of spore radius and intergill distance to predict Buller's drop radius at maximum packing. We computed average and standard deviation of spore radius and intergill distance across single individuals and placed these data on the phase space generated by our hypothesis for maximum spore packing (symbols and error bars in FIG. 4B). Whereas most parameters of our model are known (TABLE 1), α and ρ_s are not. In order to understand how the model depended on parameters, we derived an approximate formula from EQUATION 3, showing that in our model the optimal radius of Buller's drop depended only weakly on these free parameters. Indeed, when $y_{pack} < 1$, we could expand EQUATION 3 to leading order, i.e., neglecting the smallest terms in the equation. In EQUATION 3, we neglected $y_{pack}{}^3 \ll 1$ and $y_{pack}{}^3 \ll \beta$, to obtain

$$R_B \sim d\sqrt{\frac{27\rho_a}{8\alpha\rho_s}\frac{\nu^2\rho_a}{R_s\gamma}} \qquad (4)$$

This compact formula explicitly connected the radius of Buller's drop at maximum packing with the parameters of the problem. Particularly, it showed that Buller's drop radius at maximum packing depended on $(\alpha\rho_s)^{-1/2}$. For the range of variation reported in the literature (see TABLE 1), $\alpha\rho_s = 0.4\ g/cm^3$ to $1.9\ g/cm^3$, and plugging these values as well as data collected in this study in our model, we predicted that at maximum packing $< y_{\text{this study}} > = 50\%$ to 23%. Importantly, the observed value of y from the literature is within this range of variation: $< y_{\text{literature}} > \sim 32\%$, which supports the hypothesis of maximum packing. The value of the fitting parameters for which the predicted Buller's drop radius for maximum packing averaged over our collected data fits the observed value, $< y_{\text{this study}} > = < y_{\text{literature}} > = 32\%$, is $\alpha\rho_s = 0.9 g/cm^3$. For the eight species analyzed in

this study, we found a standard deviation of 12%. A data set of Buller's drop radius, spore radius, and intergill distance measured on the same specimen is needed to further confirm the hypothesis of maximum packing.

Scaling of Buller's drop radius with intergill distance.— Buller's drop is often assumed to scale *proportionally* with spore size (Fischer et al. 2010b), and published data shown in FIG. 3B corroborated this assumption (although note that only 3 out of 13 species in these published data correspond to gilled mushrooms). However, the assumption appears at odds with the prediction for maximum packing because EQUATION 4 implies that Buller's drop radius scales linearly with intergill distance d and with the *inverse* square root of spore radius R_s. To resolve the paradox, intergill distance must increase with increasing spore radius in the following way:

$$d \sim 0.32 \sqrt{\frac{8\gamma\alpha\rho_s}{27{\rho_a}^2\nu^2} R_s^3}$$

where we have simply plugged $R_B \sim 0.32 R_s$ into EQUATION 4 In order to convincingly prove or disprove this relationship, further data monitoring spore, drop, and gill morphologies, as well as spore density and ejection velocity, are needed.

DISCUSSION

The intricate morphologies of gilled mushrooms are hypothesized to maximize surface to volume ratios, an adaptation enabling the maximum packing of spores within a minimal investment of biomass. The hypothesis requires intergill distances to be exactly twice the horizontal range of an ejected spore: an ejected spore must both clear its natal gill and avoid lodging into the gill across from it, and assuming gills are crowded together as closely as possible (to efficiently use the space within a mushroom cap), the spore will be finely tuned to reach midway between facing gills. Intergill distances may be shaped by the reach of a spore, but because spore range is dictated by the dimension of Buller's drop and its density relative to the dimension and density of the spore, the three parameters—intergill distance, spore size, and Buller's drop size—emerge as highly interdependent in the context of maximum packing. We find that intergill distances and spore sizes from empirical observations populate a region of phase space where our model predicts that the radius of Buller's drop enabling maximum spore packing ranges from 23% to 50% of spore radius. Previously published data (Pringle et al. 2005; Stolze-Rybczynski 2009; Stolze-Rybczynski et al. 2009; Fischer et al. 2010b) suggest that Buller's drop radius scales with spore dimensions as $R_B \sim 32\% R_s$ and support the hypothesis of maximum packing. A further prediction of our model is that the linear scaling of Buller's drop and spore radii implies intergill distance must scale as $R_s^{3/2}$ within an optimally packed mushroom.

The fungi used in our analyses (FIG. 3A) do not operate at maximum ejection speed; the velocity of ejection for these spores remains well below the maximum. Whether other species operate at maximum ejection speed remains to be elucidated. This result may not be surprising because robust control of ejection speed may not contribute an obvious selective advantage. By contrast, the maximum packing of spores is expected to contribute significantly to the fitness of an individual.

More data are needed: our conclusions are based on a total of 21 species. However, the data collected to date are consistent with the hypothesis of maximum packing, confirming that Buller's drop radius is likely to be finely tuned to control range and speed. How tuning evolves, and the biomechanics underpinning ballistospory, a purely extracellular process operating in the context of fluctuating environments, remains a fascinating question for future research.

ACKNOWLEDGMENTS

We would like also to thank Sarah Swanson for all her help and discussions about confocal microscopy.

FUNDING

This work was supported by the Agence Nationale de la Recherche Investissements d'Avenir UCAJEDI ANR-15-IDEX-01, by the Centre National de la Recherche Scientifique Projet international de cooperation scientifique (PICS) "2FORECAST," by the Thomas Jefferson Fund, a program of FACE, and by the Global Health Institute at the University of Wisconsin–Madison. Research at the Huron Mountains was supported by the Huron Mountain Wildlife Foundation.

ORCID

Yen-Wen Wang http://orcid.org/0000-0002-6851-1646
Anne Pringle http://orcid.org/0000-0002-1526-6739
Agnese Seminara http://orcid.org/0000-0001-5633-8180

LITERATURE CITED

Blackwell M. 2011. The fungi: 1, 2, 3, … 5.1 million species? American Journal of Botany 98:426–438.
Buller AHR. 1909. Researches on Fungi, Vol. II. London, UK: Longmans, Green and Co. 416 p.

de Gennes PJ. 1985. Wetting: statistics and dynamics. Review of Modern Physics 57:827–863.
Fischer MW, Stolze-Rybczynski JL, Yunluan CUI, Money NP. 2010b. How far and how fast can mushroom spores fly? Physical limits on ballistospore size and discharge distance in the basidiomycota. Fungal Biology 114:669–675.
Fischer MWF, Money NP. 2010. Why mushrooms form gills: efficiency of the lamellate morphology. Fungal Biology 114:57–63.
Fischer MWF, Stolze-Rybczynski JL, Davis DJ, Cui Y, Money NP. 2010a. Solving the aerodynamics of fungal flight: how air viscosity slows spore motion. Fungal Biology 114:943–948.
Fisher MC, Henk DA, Briggs CJ, Brownstein JS, Madoff LC, McCraw SL, Gurr SJ. 2012. Emerging fungal threats to animal, plant and ecosystem health. Nature 484:186–194.
Fritz J, Seminara A, Roper M, Pringle A, Brenner MP. 2013. A natural O-ring optimizes the dispersal of fungal spores. Journal of the Royal Society Interface 10:20130187.
Hoorfar M, Kurz MA, Policova Z, Hair ML, Neumann AW. 2006. Do Polysaccharides such as dextran and their monomers really increase the surface tension of water? Langmuir 22:52–56.
Hussein T, Norros V, Hakala J, Petaja T, Aalto PP, Rannik U, Vesala T, Ovaskainen O. 2013. Species traits and inertial deposition of fungal spores. Journal Aerosol Science 61:81–98.
Kues U, Liu Y. 2000. Fruiting body production in basidiomycetes. Applied Microbial Biotechnology 54:141–152.
Kupferschmidt K. 2012. Attack of the clones. Science 337:636–638.
Liu F, Chavez RL, Patek SN, Pringle A, Feng JJ, Chen CH. 2017. Asymmetric drop coalescence launches fungal ballistospores with directionality. Journal of the Royal Society Interface 14:20170083.
McKnight KB, Roundy RO. 1991. Optimal gill packing in agaric sporocarps. Journal of Theoretical Biology 150:497–528.
Noblin X, Yang S, Dumais J. 2009. Surface tension propulsion of fungal spores. The Journal of Experimental Biology 212:2835–2843.
Pennisi E. 2010. 1000 genomes project gives new map of genetic diversity. Science 29:574–575.
Phillips R. 1991. Mushrooms of North America. Boston, Massachusetts: Little, Brown & Company. 319 p.
Pringle A, Patek S, Fischer M, Stolze J, Money N. 2005. The captured launch of a ballistospore. Mycologia 97:866–871.
Schmitz J. 1843. Beitrage zur Anatomie und Physiologie des Schwämme. Linnaea 17:437.
Schoch CL, Seifert KA, Huhndorf S, Robert V, Spouge JL, Levesque CA, Chen W, Fungal Barcoding Consortium. 2012. Nuclear ribosomal internal transcribed spacer (ITS) region as a universal DNA barcode marker for Fungi. Proceedings of the National Academy of Sciences of the United States of America 109:6241–6246.
Stokes GG. 1851. On the effect of internal friction of fluids on the motion of pendulums. Transactions of the Cambridge Philosophical Society 9:8–106.
Stolze-Rybczynski JL. 2009. Biomechanics of spore discharge in the basidiomycota [PhD dissertation]. Oxford, Ohio: Miami University. 112 p.
Stolze-Rybczynski JL, Cui Y, Henry M, Stevens H, Davis DJ, Fischer MW, Money NP. 2009. Adaptation of the spore discharge mechanism in the Basidiomycota. PLoS ONE 4: e4163.
Wang H, Qi M, Cutler AJ. 1993. A simple method of preparing plant samples for PCR. Nucleic Acids Research 21:4153–4154.
Webster J, Davey RA, Ingold CT. 1984. Ballistospore discharge in *Itersonilia perplexans*. Transactions of the British Mycological Society. 82: 13–29.
Webster J, Davey RA, Turner JCR. 1989. Vapour as the source of water in Buller's drop. Mycological Research 93:297–302.
Webster J, Davey RA, Smirnoff N, Fricke W, Hinde P, Tomos D, Turner JCR. 1995. Mannitol and hexoses are components of Buller's drop. Mycological Research 99:833–838.